FULL PAPER

Unusually High Optical Transmission in Ca:Ag Blend Films: High-Performance Top Electrodes for Efficient Organic Solar Cells

Sylvio Schubert, Lars Müller-Meskamp, and Karl Leo*

Highly transparent electrodes are demonstrated based on thermally evaporated calcium:silver blend thin–films, which show unusually high transmission well above the expectations from bulk material properties and thin film optics. These electrodes exhibit a low sheet resistance of 27.3 Ω/□, combined with an extraordinarily high mean transmittance of 93.0% in the visible spectral range (σ_{dc}/σ_{opt} = 186.7), superior to the commonly used inorganic electrodes made from indium tin oxide (ITO). Additionally, the metal blend electrode is flexible, showing a constant sheet resistance down to a bending radius of 10 mm and can be employed on top of organic devices without causing damage to the organic material. The spontaneously formed unique microstructure of a polycrystalline Ag network with randomly distributed nanoapertures, surrounded by a calcium shell, enables broadband transmittance enhancement due to amplified plasmonic coupling. Consequently, top-illuminated organic solar cells using such metal blend electrodes achieve a power conversion efficiency of 7.2% (which defines a new record for top illuminated organic solar cells) and even exceed the efficiency of similar bottom-illuminated reference solar cells (6.9%) employing common ITO electrodes.

1. Introduction

Transparent conductive electrodes are a key component of future optoelectronic devices. The current benchmark in the field of transparent conductors is indium tin oxide (ITO), combining excellent optical and electrical properties with an average transmittance in the visible spectral range over 90% and a sheet resistance down to 11 Ω/□.[1] However, due to its brittleness[2] and the scarcity of indium,[3] ITO replacements, e.g., conductive polymers such as PEDOT:PSS,[4] silver nanowires,[5,6] ultra-thin metal films,[7,8] carbon nanotubes,[9–11] or graphene[11–15] are subject of intense research. In the long term, the most promising application for such electrodes might be organic photovoltaics (OPV). Continuous advances in materials and device concepts have recently led to efficiencies of up to 12%.[16] Moreover, OPV shows the potential for fast and cost-efficient roll-to-roll production[17] of flexible, semitransparent, and lightweight devices,[14,15] offering attractive properties for novel applications. For that purpose, flexible and mechanically stable substrates such as opaque metal foils are desired, requiring a device architecture with transparent top electrode. For such applications, ITO is not suitable due to the high deposition temperature and damage of the underlying devices.[18,19]

Here, we investigate ultra-thin calcium:silver (Ca:Ag) blend layers as flexible, transparent, conductive electrode, and its integration as top electrode for highly efficient organic photovoltaic cells. In contrast to pure silver layers which tend to form isolated nuclei (Volmer-Weber growth mode), leading to non-conductive films[20] and strong particle plasmon absorption,[21] a Ca:Ag blend electrode based on an aluminum seed layer[7] shows no island formation which enables highly conductive films down to a thickness of 4 nm. As frequently suggested in literature, the metal layers are embedded between two dielectric layers to increase electrode transparency[21–27] and solar cell lifetime.[27] In addition, structural investigations reveal a spontaneously forming nanoscale material separation of Ca and Ag and a nanohole formation in the layer. This amplifies the excitation of surface plasmon polaritons and strongly increases the film transmittance by the coupling of plasmons on the front- and backside of the metal layer. Such a mechanism is possibly similar to previously reported extraordinary optical transmission for larger aperture arrays in thicker layers,[28–30] but enables a spectrally broad transmittance enhancement. Consequently, the electrode performance and the solar cell efficiency can be significantly improved compared to state-of-the-art metal electrodes and even to ITO.

2. Electrode Characterization

Figure 1a depicts the schematic stack design of the electrode-only samples. The transparent doped hole-transport layer BF-DPB:NDP9 and MoO_3 are employed to mimic the complete solar cell stack and to ensure similar growing behavior. A 1 nm thick seed layer[7] plus 1 nm of pure silver are used to influence the microstructure of a Ca:Ag blend thin film in the mixing ratio of 2:1. Alq_3 serves as antireflection coating for

S. Schubert, Dr. L. Müller-Meskamp, Prof. Dr. K. Leo
Institut für Angewandte Photophysik
Technische Universität Dresden
George-Bähr-Straße 1, 01069, Dresden, Germany
E-mail: sylvio.schubert@iapp.de

DOI: 10.1002/adfm.201401854

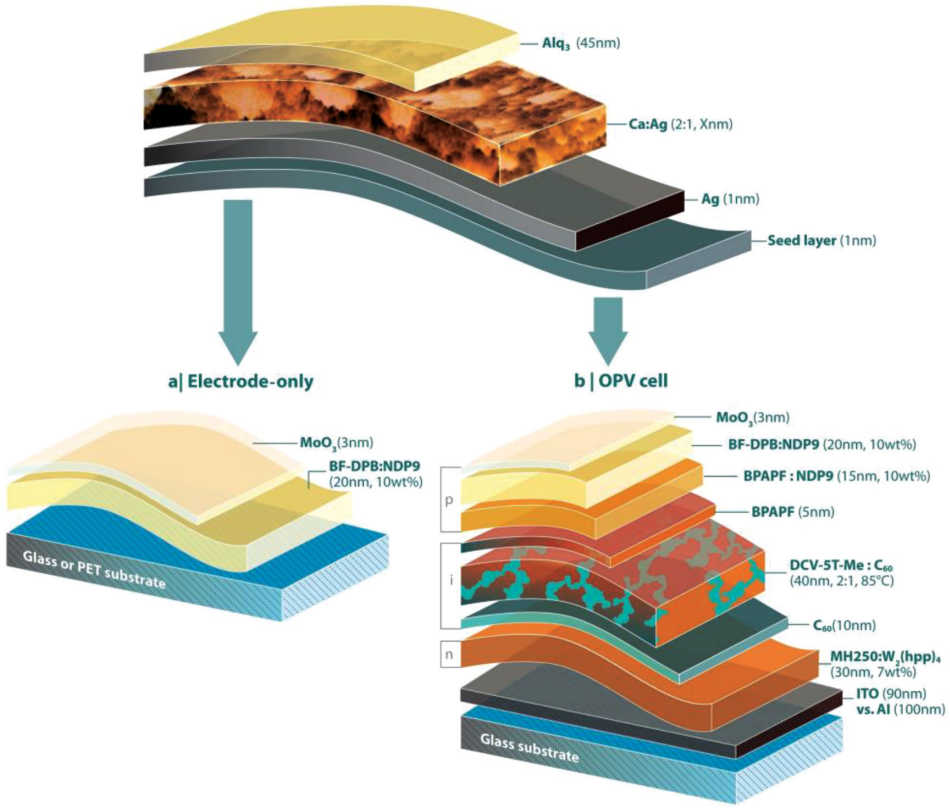

Figure 1. Sample stack design. a) Electrode-only samples and b) complete n-i-p small molecule organic solar cells. The electrode-only samples represent the upper layers of the solar cell and are used to study microstructure, conductivity, and optical properties.

all metal electrodes. A detailed material description is provided in the experimental section. To optimize the electrode performance, we varied the seed layer material and the blend layer thickness. **Figure 2**a shows the transmittance spectra and corresponding sheet resistances of 8 nm thick Ca:Ag electrodes, depending on the employed seed layer (1 nm of gold, calcium, aluminum, or no seed). For comparison, the transmittance and sheet resistance of our lab-standard ITO, a 10 nm thick pure Ag electrode, and a successively deposited bi-layer of 3 nm thick pure silver and 5 nm thick pure calcium are depicted. For pure silver films, we recently found that a gold seed layer can significantly improve the thin film microstructure and optoelectronic performance.[7] Thus, the single Ag and the Ag/Ca bi-layer is deposited on an additional 1 nm thick Au seed. Note that all transmittance spectra presented in this article are not substrate corrected.

Even without any seed layer, the Ca:Ag blend electrode shows a high mean transmittance T_{vis} of 79.5% in the visible spectral range between 400 nm and 800 nm. Particularly in the near infrared region, unusually high transmittance is observed, which cannot be achieved by a simple successive deposition of two Ag and Ca layers with a similar amount of material (3 nm Ag and 5 nm Ca, respectively). We ascribe this very high transparency to a plasmonic coupling effect similar to extraordinary optical transmission,[28–30] as discussed later. The sheet resistance of the metal blend layer is 283.3 Ω/□, much lower than the 3000 Ω/□ of the planar stacked sample. However, it is still one order of magnitude higher than for ITO, limiting its usability with respect to large area applications. Introducing a gold seed layer reduces the transmittance by approximately 10% without changing the conductivity of the film, which suggests an unfavorable microstructure of the Ca:Ag blend and contradicts the findings for pure Ag electrodes.[7] Also the calcium seed slightly reduces the electrode transmittance, but improves its sheet resistance to 89.2 Ω/□. In contrast, the aluminum seed layer causes the formation of a very transparent and conductive blend film, exhibiting a low sheet resistance of 27.3 Ω/□ and a mean transmittance of 84.3%. Such an electrode system exceeds the performance of state-of-the-art metal[31,32] and metal blend[33] electrodes and is even superior to the ITO used in our lab (R_S = 32 Ω/□, T_{vis} = 83.0%). Subtracting the refractive index mismatch losses at the glass interfaces leads to a transmittance of the solitary Ca:Ag electrode system of T_{vis}^* = 93.0%. In the spectral range between 500 nm and 800 nm, where the photon flux of the sun has its maximum, the Ca:Ag based electrode exceeds the transmittance of ITO by up to 6.3%, pointing out the great potential of this electrode in combination with a solar cell. With a total thickness (Al and Ag seeds + blend layer) of 10 nm, the Ca:Ag electrode presented here shows a similar sheet resistance compared to a pure 10 nm thick silver electrode, while having a drastically improved transmittance. The figure of merit σ_{dc}/σ_{opt}, introduced by Gruner et al.,[34] is 103.1 for the pure silver layer (10 nm), poor 0.6 for the Ag(3 nm)/Ca(5 nm) stack, 125.2 for ITO, and remarkable 186.7 for the optimized Ca:Ag

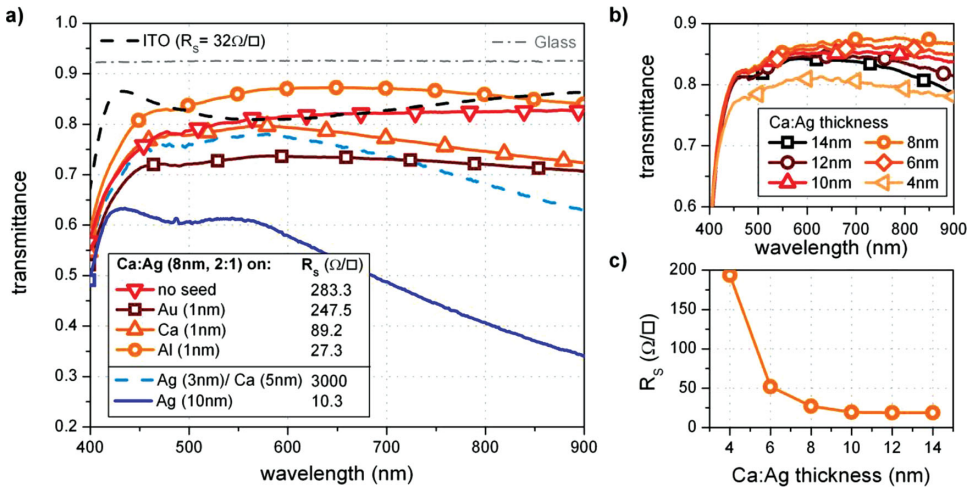

Figure 2. Electrode performances on glass/p-doped BF-DPB (20 nm)/MoO_3 (3 nm) substrates and with Alq_3 (45 nm) capping layer a) Transmittance and sheet resistance R_S of 8 nm thick Ca:Ag layers (2:1) deposited on 1 nm of varying seed layer: Ca, Au, Al, or no seed. For comparison, samples with 10 nm of pure Ag and successively deposited 3 nm Ag plus 5 nm Ca (same amount of material as in the blend) are depicted. To guarantee a reliable performance, both Ag films are deposited on 1 nm Au as seed layer.[7] 90 nm ITO on glass serves as reference. b) Transmittance of Ca:Ag electrodes of varying thickness, using an Al seed layer. c) Corresponding sheet resistance of the Ca:Ag electrodes depending on the layer thickness. None of the transmittance graphs are substrate corrected.

electrode system (8 nm, 2:1, Al seed). Additionally, replacing two thirds of the noble and expensive metal silver with the low cost material calcium leads to a significant reduction of material costs compared to bare silver or ITO.[3]

Figure 2c and 2d give additional information about the thickness dependency of the metal blend electrode (from now on always deposited on an Al seed layer) concerning transmittance and sheet resistance, respectively. Although the 4 nm Ca:Ag blend represents the thinnest layer in this comparison, it shows the lowest transmittance, suggesting a partially discontinuous film morphology. Isolated metal clusters can lead to the excitation of localized surface plasmons, which represent a loss mechanism for the transmission of light.[7,21] A partially discontinuous film is also indicated by the rather high sheet resistance of 193.6 Ω/□. With increasing layer thickness, the film completely coalesces and the transmittance is increased, showing an optimum at 8 nm. Further material deposition leads to a reduced transmittance, as known from pure metal films. However, the decrease in transmittance with increasing layer thickness is uncommonly small (resulting in T_{vis} = 81.6% even for 14 nm Ca:Ag) and cannot be explained by the Lambert-Beer law. Particularly in the red and near infrared region where the extinction coefficients of the single metals are high, an excellent transmittance is observed for all Ca.Ag electrodes, suggesting an additional transmission phenomenon, only weakly dependent on the layer thickness. A comparable behavior is known only from extraordinary optical transmission of periodic aperture arrays in opaque metal films.[28–30] The sheet resistance continuously decreases with increasing layer thickness up to 10 nm and then saturates at values of around 18 Ω/□. This weak dependency of T_{vis} and R_S on the precise layer thickness is highly beneficial for a potentially fast and large-scale electrode production and results in excellent yield and reproducibility of the Ca:Ag electrodes. It is known that calcium is a highly reactive material and unstable in air or moisture. However, an ultra-thin oxide layer on both sides of the metal blend layer can sufficiently stabilize the electrodes,[27] even without an additional encapsulation (see below).

3. Structural Investigations

In order to obtain further insight and a better understanding of the mechanisms behind the excellent electrode properties, a series of microstructure investigations of the Ca:Ag electrode system has been carried out. **Figure 3**a depicts a transmission electron micrograph (TEM) of an electrode stack as described in Figure 1a but on a carbon coated copper grid substrate. A contrast rich micrograph can be seen, displaying not a smooth but nanoscale structured film morphology with bright and randomly distributed features of 5 nm – 40 nm in diameter. The cross sectional TEM of the same sample shown in Figure 3e reveals that the structures appear only in the Ca:Ag layer, hinting at a material or phase separation. Since the lamella for the cross sectional TEM measurement is cut by focused ion beam (FIB) to a thickness of 100 nm, being significantly larger than the maximum feature size, it is not possible to discover entire holes in Figure 3e. Dark colored nanoflakes (indicating a dense and crystalline material) are closely packed. In between, some brighter (low density) areas are visible. The sample is also probed by atomic force microscopy (AFM), showing a similar structure size as in the TEM and a low root mean square roughness of 1.2 nm (see Figure 3b). As the nominal Ca:Ag layer thickness is only 8 nm compared the maximum height difference in the AFM image of 13.1 nm, we assume the bright areas to be empty holes in the blend film, reaching from the top to almost the bottom. Consequently, the Ca:Ag electrode spontaneously forms a metal network, including randomly distributed nanohole features and probably partially crystallized grains. That result is strongly supported by energy filtered TEM measurements, which will be discussed later. Figure 3c shows the electron diffraction pattern of the Ca:Ag contact measured with the TEM. The visible rings

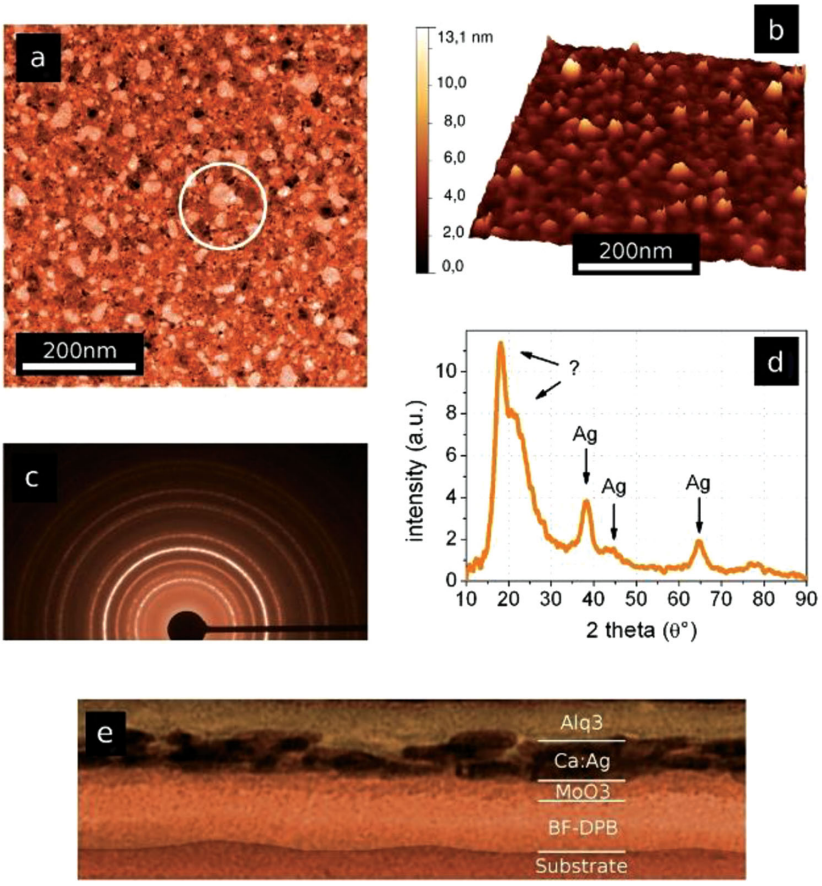

Figure 3. Structural investigations. In all subfigures, a Ca:Ag electrode (2:1, 8 nm) using an Al seed layer is probed. a) Top view transmission electron micrograph. b) Atomic force micrograph. c) Electron diffraction pattern. d) X-Ray diffraction pattern. e) Cross sectional transmission electron micrograph.

indicate a polycrystalline film structure. Due to the variety of possible materials (Ca, Ag, Al, their oxides and alloys, MoO_3, or organic compounds), it is difficult to assign the ring radii for a particular material or material system. However, there are hints on nanocrystalline Ag, AgCa, Ag_3Ca_5, and also CaO_2 phases in the blend layer. Possibly, a significant part of the Ca in the film already oxidizes during deposition, which might explain the reasonable stability of the Ca:Ag electrode. Additional X-ray diffraction measurements shown in Figure 3d confirm the presence of a crystalline phase of pure silver, but pristine calcium could not be detected. Although the prominent peaks at low diffraction angles cannot be assigned unambiguously, they suggest material phases with a large unit cell (e.g., Ag_7Ca_9 or various metal oxides).

Further investigations of the network microstructure are carried out by energy filtered TEM. Since electrons are subject to a characteristic, material dependent energy attenuation while passing through the sample, this technique allows a spatially resolved material analysis on a nanometer scale. **Figure 4** depicts scanning EF-TEM images of the Ca:Ag blend electrode for the characteristic energy losses of Ag, Ca, C, or O interaction. Silver is forming a nanoporous network with many holes inside, but without any separated clusters. The formation of crystalline silver percolation paths in the electrode layer can explain the excellent conductivity even at low film thickness. In

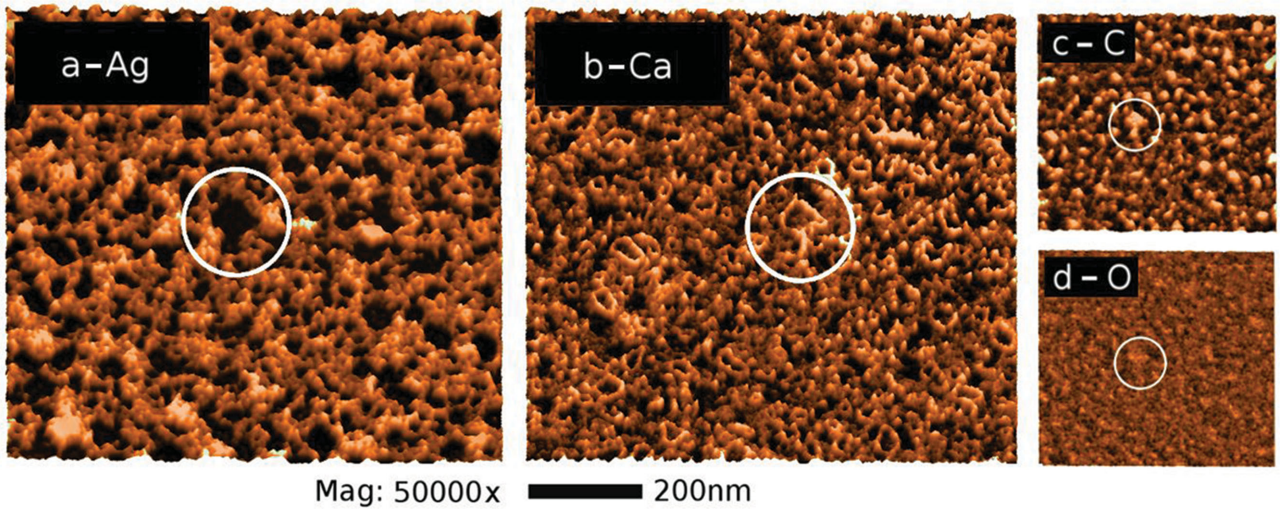

Figure 4. Energy filtered transmission electron microscopy. Scans of an 8 nm thick Ca:Ag blend electrode (2:1) on Al seed, filtered by the characteristic energy losses for an electron beam interaction with a) silver, b) calcium, c) carbon, and d) oxygen atoms. A bright area (strong signal) indicates the presence of the actual material. The white circle highlights a characteristic area.

contrast, calcium is strongly enriched at the edges of the silver mesh. Probably, the low surface energy of the initially deposited Ca (or CaO_2) is unfavorable for further silver deposition and subsequently deposited silver particles diffuse to calcium free regions.[7] Similar processes might force the Ca to agglomerate at the Ag interface of higher surface energy, suggesting a growth model which most likely explains the material separation, the Ag network structure, as well as the hole formation. The carbon signal in Figure 4c represents the inverse of the Ag distribution. Since carbon is present along the entire substrate and capping layer but the signal is attenuated when other materials are in the trajectory of the electrons, it proves the assumption that the holes in the metal layer are empty and extend almost down to the bottom. In contrast, the signal of oxygen is homogeneous and low, hinting at a weak oxidation of the entire sample surface.

Such spontaneously formed silver nanomeshes enable an excitation of surface plasmon polaritons (SPPs). Since the metal thickness is extremely low (~10 nm), a strong coupling between SPPs on the front- and backside of the electrode is expected. For periodically patterned nanoaperture arrays in optically thick metal films, extraordinary optical transmission (EOT) in a very narrow spectral range caused by plasmonic coupling has been observed.[28–30] However, the apertures in the Ca:Ag blend films presented here are irregularly shaped, randomly distributed, and much smaller than the usually reported FIB milled holes of a few 100 nm (partially even smaller than the resolution limit of the FIB milling technique at all). Thus, a novel broadband transmission enhancement effect beyond the expectations from bulk material properties and thin film optics might be observed here. Probably, an improved coupling of upper and lower side plasmons could explain the extraordinarily high mean transmittance of the Ca:Ag network, particularly in the red and near-infrared region, where the optical constants of Ca and Ag would suggest a lower transmittance.

4. Electrode Flexibility

To study its flexibility, the Ca:Ag blend electrode is deposited on a plastic sheet (PET, pre-coated with 20 nm BF-DPB:NDP9 and 3 nm of MoO_3) and systematically bent, while the sheet resistance is measured for decreasing bending radii (see **Figure 5**). A SEM picture of the unbent sample at a magnification of 10000 × shows a smooth, homogeneous film. The initial sheet resistance of the unbent electrode on PET is R_S = 29 Ω/□. First, the sample is bent 50 times with a bending radius of 65 mm and the electrode subject to tensile stress. Then, the sheet resistance is measured. This procedure is repeated with successively decreasing bending radius. Down to bending radii of 10 mm, no change in R_S is detectable, showing the great potential of these electrodes for roll-to-roll production. A further reduction of the bending radius to 0.7 mm results in a slightly increased sheet resistance to 42 Ω/□. Finally, at a bending radius of 125 µm, which equals the thickness of the polymer substrate, an increase to R_S = 122 Ω/□ can be observed. The SEM reveals a formation of several long cracks in the film, perpendicular to the bending direction, hindering an efficient charge transport. However, the ductile properties of silver prevent a total failure even at this extreme stress.

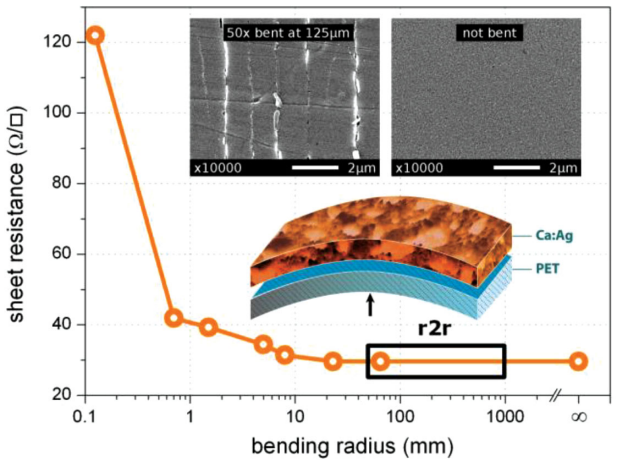

Figure 5. The cumulative bending test shows the sheet resistance of a Ca:Ag electrode (2:1, 8 nm, Al seed) on PET foil as a fiction of the bending radius. The sample is bent 50 times for each radius. Two scanning electron micrographs reveal a formation of long cracks perpendicular to the bending direction, causing a significant increase in sheet resistance. The black frame highlights the range of bending radii typically used for roll-to-roll (r2r) production.

5. Organic Solar Cells with Ca:Ag Top Electrodes

The optimized Ca:Ag (2:1, 8 nm, Al seed) blend electrode is successfully applied as top electrode in highly efficient small molecule n-i-p solar cells. Such a top-illuminated device (see Figure 1b) is compared to an identical bottom-illuminated reference sample with a standard ITO bottom electrode and an opaque 100 nm Al top electrode. Four identical samples of each device type are fabricated to ensure reproducible results. Since process- and measurement-related relative sample-to-sample variations are lower than 5%, the device characteristics of the best performing sample are shown in **Figure 6**a and summarized in the legend, while the measurement ranges are given only for the efficiency.

The open circuit voltage (V_{OC}) of an n-i-p device is determined by the energy levels in the bulk heterojunction and therefore similar for both devices at 0.95 V. As suggested by the transmittance measurements, slightly more photons can enter the photoactive layers of the solar cell through the metal blend contact, resulting in an increased short circuit current density (j_{SC}) of 12.31 mA/cm^2, compared to 12.16 mA/cm^2 for the ITO cell. The series resistance of the devices (determined from the linear slope in forward direction) is strongly reduced from 56.7 Ω to 38.2 Ω by introducing the transparent metal blend electrode, indicating that the excellent results of the electrode-only samples are conserved on top of the complete solar cells. The reduced resistance is particularly advantageous for large scale OPVs, where its influence on device performance is more pronounced. Higher electrode conductivity also enables an improved charge carrier collection and reduced recombination, reflected in an increased fill factor (FF) from 59.64% to 61.91%. Taking all parameters into account, a remarkable power conversion efficiency of 7.2% is achieved for top-illumination through the Ca:Ag electrode, which is an improvement compared to the 6.9% of the bottom-illuminated (also optimized) standard device on ITO. This is the highest reported efficiency

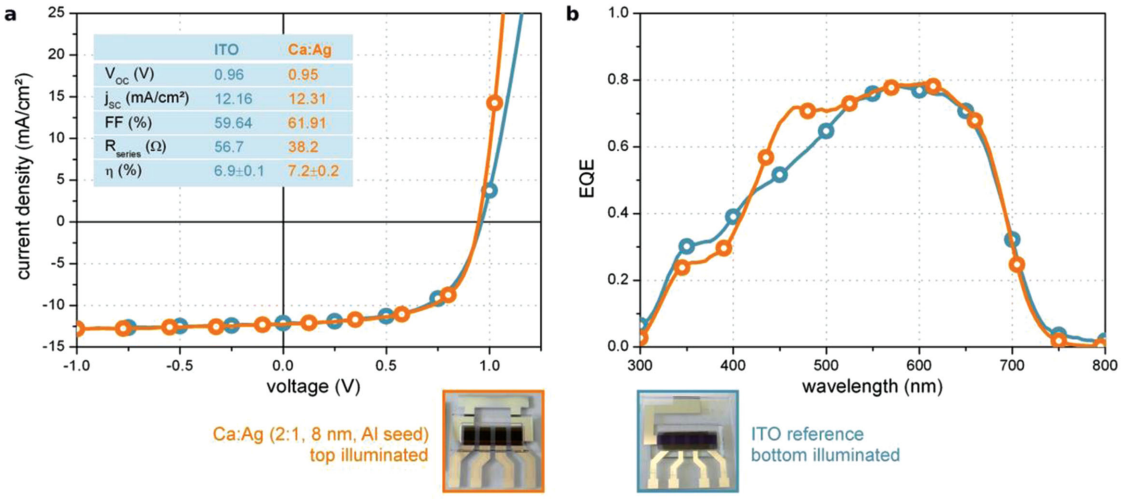

Figure 6. a) Current–voltage curves and finger prints measured under AM1.5G illumination (100 ± 1 mW/cm^2). The top-illuminated devices with flexible Ca:Ag top electrode (2:1, 8 nm, Al seed) are compared to conventional bottom sensitive devices with ITO bottom contact. For the efficiency, the measurement range of four identical solar cells for each sample type is shown. b) External quantum efficiency (EQE) of the same samples, measured at short circuit conditions without additional bias illumination. There is no shift in the absorption peaks of DCV-5T-Me (at 600 nm) or C_{60} (at 350 nm), hinting at a similar photon flux distribution in the top and bottom devices. At 480 nm, a cavity mode appears for the device using the metal contact.

for a top-illuminated small molecule solar cell so far. Combining improved scalability due to the low sheet resistance and enhanced processing due to flexibility and applicability as top contact, the Ca:Ag blend electrode is not only a promising alternative to ITO, but clearly outperforms the current state-of-the-art. In particular, devices on opaque substrates and flexible or transparent devices can be prepared without introducing any drawbacks (additional data for transparent organic solar cells is provided in the supplementary).

Figure 6b shows the external quantum efficiency (EQE) of the bottom- and top-illuminated solar cells, recorded at short circuit conditions. Both devices show a high EQE up to 80% at a wavelength of 600 nm. The peaks are not shifted for the different illumination directions, suggesting a similar photon flux distribution in both devices, as intended by using the same film thickness for the electron and hole transport layers. However, in the absorption range of DCV-5T-Me[35] (between 400 nm and 700 nm), the top-illuminated cell exhibits a slightly higher EQE, according to the improved electrode transmittance. Additionally, at 480 nm a cavity mode appears in the top-illuminated cell, which is amplified by a higher reflectivity and different optical constants of the metal blend compared to dielectric ITO. Since the absorption probability of light which is trapped in such a cavity is increased, the EQE is higher, the short circuit current is enhanced, and finally the power conversion efficiency is improved. The cavity effect could be particularly advantageous for complementary tandem or multi-junction devices.

6. Stability and Lifetime

In **Figure 7**a, the normalized power conversion efficiency of a top illuminated solar cell with Ca:Ag top electrode is shown as a function of time and compared to a standard bottom

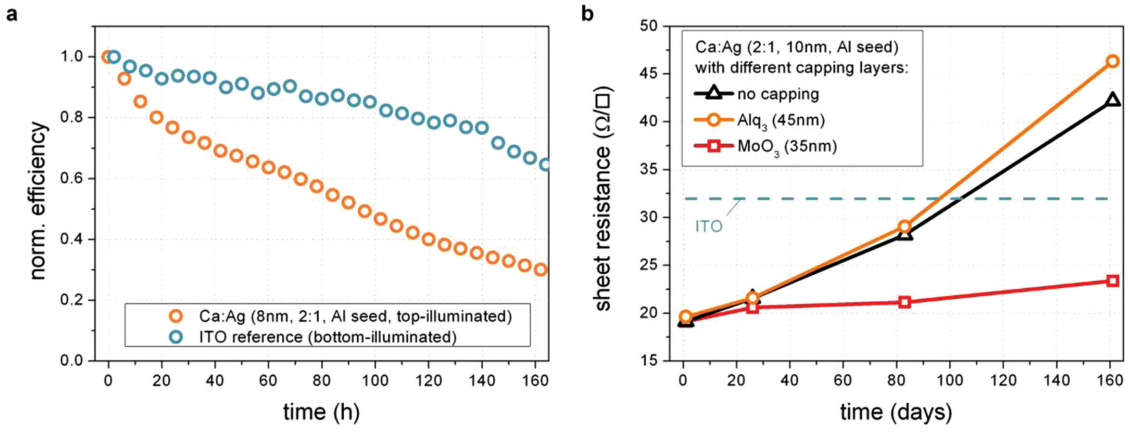

Figure 7. a) Comparison of the stability of two glass-glass encapsulated organic solar cells as a function of time, using either Ca:Ag or ITO as transparent top or bottom electrode, respectively. Both devices have been exposed to identical and constant aging conditions: ambient air, continuous AM1.5G illumination (100 mW/cm^2), and 65 ± 1 °C. b) Long term stability of the Ca:Ag electrode system in air, using different capping layers.

illuminated cell on ITO. The devices are encapsulated by a glass lid and the stacks are identical as described in Figure 1. Typically, the solar cell lifetime is defined as the time it takes for the efficiency to decay to 80% of its initial value (T_{80}). While the ITO reference cell is rather stable, showing a T_{80} of 108 h under continuous illumination, the cell with Ca:Ag top electrode rapidly degrades at the beginning of the measurement, leading to a low T_{80} of only 19 h. Later, the degradation rates are comparable. Since the organic layer sequence is identical for both devices, the accelerated degradation is assigned to the Ca:Ag electrode or the interface between this electrode and the organic stack. However, it is known from literature that ultrathin metal electrodes are prone to rapid degradation, because of an unfavorable surface to volume ratio.[27,36,37] Thus, the device lifetimes achieved here are in the expected range and not drastically decreased because of the utilization of the highly reactive calcium in the electrodes. The Ca:Ag electrode system is covered by a 45 nm thick Alq_3 capping layer. This organic capping is not able to protect the electrodes (see Figure 7b), leading to a constantly increasing sheet resistance as a function of storage time in air.

However, we could previously show that a thin metal electrode can be significantly stabilized by an oxide sandwich surrounding the metal.[27] Applying this concept to the Ca:Ag layer leads also to an improved electrode stability and a low increase in sheet resistance R_S from 19.1 Ω/□ to 23.4 Ω/□ after storing 165 days in ambient atmosphere, without an encapsulation. Note that the transmittance of all Ca:Ag electrodes stays almost constant over time. We assume that an additional oxide capping could also stabilize the organic solar cells presented in Figure 7a and passivate the Ca:Ag electrodes for further degradation.

7. Conclusion

We have investigated thin Ca:Ag blend films which can be employed as excellent transparent and flexible top electrodes for highly efficient small molecule organic photovoltaic cells. In contrast to conventional semitransparent metal contacts with similar sheet resistance, the electrode transmittance is drastically increased while the material costs are reduced. Embedded between two dielectric layers and in combination with a 1 nm thick aluminum seed layer, a Ca:Ag electrode with a thickness of 8 nm and a blending ratio of 2:1 exhibits an extraordinarily high mean transmittance of visible light between 400 nm and 800 nm wavelength T_{vis} of 84.3% (93.0% after substrate correction) and a sheet resistance R_S of 27.3 Ω/□, both superior to our lab ITO (R_S = 32 Ω/□, T_{vis} = 83.0%). The σ_{dc}/σ_{opt} ratio of the optimized metal blend electrode reaches 186.7. Additionally, the presented electrode system is highly flexible, with a constant conductivity down to a bending radius of 10 mm, showing the great potential of these metal electrodes for fast, cost-efficient, reliable, and high-purity roll-to-roll processing. The origin of the superior performance is examined by microstructure studies. TEM measurements reveal that – driven by a phase segregation – the silver in the blend electrode forms a partially crystalline network. Randomly distributed nanoapertures in the film enable amplified plasmonic coupling, similar to EOT, but leading to a unique broadband transmittance enhancement. Organic solar cells employing Ca:Ag films as top electrode show superior current generation and charge collection and achieve 7.2% efficiency, exceeding the 6.9% efficiency of bottom-illuminated reference solar cells with conventional ITO electrodes. The stability of the Ca:Ag films is comparable to other ultrathin metal electrodes, despite the high amount of Ca in the layer. It is shown that the metal blend electrodes investigated in this study can replace ITO and fill the lack of high performance flexible, transparent, conductive top electrodes, which are particularly interesting for roll-to-roll processed organic photovoltaic cells, OLEDs, semitransparent devices, devices on opaque substrates, or photonic devices.

8. Experimental Section

Sample Preparation: All samples shown in this publication are fabricated in a custom-made vacuum system (K.J. Lesker, UK) by thermal (co-)evaporation at a base pressure of 10^{-7} mbar, using shadow masks. The glass (Corning Eagle XG, 1.1 mm, Thin Film Devices, USA), PET (Melinex ST 504, 125 µm, DuPont Teijin Films, USA), and ITO (Thin Film Devices, USA) substrates are carefully cleaned with NMP, ethanol, and oxygen plasma before being transferred into the vacuum chamber. During one processing run of 36 samples, the intentional variation of specific layers or parameters is possible for specific samples, while all other layers are deposited under identical conditions. This allows to include reference samples, which can be used for direct comparison within one run, and comparisons for equal stacks in different runs to validate processing over time. In case of the samples shown in this paper, only the seed layer material and the film thickness of the Ca:Ag electrode are varied and its influence is investigated. The sample yield was >98%. All layer thicknesses are monitored with calibrated quartz crystal microbalances; in case of the very thin layers in the range of 1 nm, the layers are probably neither smooth nor closed, so the thickness given here has to be interpreted in terms of nominal or equivalent thickness, indicating the amount of material on the sample. The small molecule organic solar cells presented here are n-i-p type, i.e., the intrinsic absorber (i) is embedded between dedicated, doped electron (n) and hole (p) transport materials. The complete stack is shown in Figure 1. As cathode, either an opaque metal layer of 100 nm aluminum or a 90 nm thick, pre-structured layer of indium tin oxide (Thin Film Devices, USA) is used. ITO acts as transparent contact for bottom-illuminated reference devices which utilize the 100 nm aluminum layer as counter electrode on top. The high reflectivity of aluminum creates a cavity in both (bottom- and top-illuminated) devices which enables improved light absorption. As electron transport layer, 30 nm of N,N-Bis(fluoren-2-yl)-naphthalenetetracarboxylic diimide (MH250, produced in house) n-doped with 7 wt% of tetrakis(1,3,4,6,7,8-hexahydro-2H-pyrimido[1,2-a]pyrimidinato)ditungsten (II) ($W_2(hpp)_4$, Novaled AG, Germany) are employed. 10 nm intrinsic C_{60} (BuckyUSA, USA; purified by CreaPhys GmbH, Germany) serves as electron transport layer and acceptor followed by a 40 nm thick bulk heterojunction consisting of C_{60} and a methylated DCV-5T derivative[35] (2,2′-((3″,4″-dimethyl-[2,2′:5′,2″:5″,2‴:5‴,2⁗-quinquethiophene]-5,5⁗-diyl)-bis(methanylylidene))dimalononitrile, Synthon, Germany) simultaneously evaporated with a weight ratio of 1:2. During evaporation of the bulk heterojunction, the substrate is heated to 85 °C. Next, 5 nm of intrinsic 9,9-bis[4-(N,N-bis-biphenyl-4-yl-amino)phenyl]-9H-fluorene (BPAPF, Lumtec, Taiwan; purified in house) is deposited. For efficient hole transport and injection, 15 nm of BPAPF and 20 nm of N,N′-((Diphenyl-N,N′-bis)9,9,-dimethyl-fluoren-2-yl)-benzidine (BF-DPB, Sensient AG, USA) both doped with 10 wt% NDP9 (Novaled AG, Germany) are deposited, followed by 3 nm molybdenum(VI)oxide (MoO_3, sigma-aldrich, USA, 99.99% purified). The MoO_3 layer prevents the interpenetration of metal and organic material during the subsequent

electrode deposition process and leads to improved hole collection properties.[27] A gold (Au), calcium (Ca), or aluminum (Al) film of only 1 nm thickness combined with an additional 1 nm of silver (Ag) acts as seed layer for the subsequently deposited calcium:silver blend layer (of varying thickness), which is used as anode. For good charge carrier extraction, forming Ohmic contacts, 1 nm of pure NDP9 or $W_2(hpp)_4$ are deposited at the interfaces between metal top electrode/BF-DPB and bottom electrode/MH250, respectively. Finally, a capping layer of 60 nm tris-(8-hydroxy-quinolinato)-aluminum (Alq_3, TCI Europe, Belgium) is deposited to reduce reflectance and increase transmittance of the metal electrode. All organic materials except the dopants and DCV-5T-Me have been purified at least twice by vacuum gradient sublimation. Note that both transport layers surrounding the photoactive bulk heterojunction have the same total thickness of 40 nm each, ensuring a similar optical field distribution in the devices for top- and bottom-illumination. Glass is used as substrate to guarantee reliable handling, sample processing and a good comparability to the ITO based reference samples. Since the bottom electrode is an opaque aluminum film, the performance of the top-illuminated solar cells is expected to be comparable also on other sufficiently planarized substrates, e.g., flexible metal foils or polymer webs. The completed solar cells are encapsulated with a transparent encapsulation glass, fixed by UV-hardened epoxy glue, in a nitrogen glovebox attached to the vacuum chamber. The photoactive active area of the organic solar cell is 6.44 mm^2, as defined by the overlap of bottom and top electrode. Additional "electrode-only" samples consisting of a simpler stack design – Substrate (Glass or PET)/p-doped BF-DPB (20 nm)/MoO_3 (3 nm)/seed layer (1+1 nm)/Ca:Ag blend (mixing ratio 2:1, 4 nm-14 nm)/Alq_3 (45 nm) – but larger area of 20 × 20 mm^2 are fabricated and characterized by optical, electrical and microstructure measurements. Since the deposition of such thin layers is very substrate-dependent, the oxide and metal layers are not directly evaporated onto glass but on 20 nm p-doped BF-DPB, which is exactly the same layer below the electrode as it is used in the organic solar cells. Thus, the growth of oxide and metal is decoupled from the glass substrate and exhibits similar growth conditions as on top of the complete organic solar cell.

Characterization: Current–voltage measurements of the OPV cells are carried out under ambient conditions using a source measurement unit (SMU 2400 Keithley, USA) and simulated AM 1.5G sun light (16S-150 V.3 by Solar Light Co., USA) taking spectral mismatch into account. The illumination intensity is kept at (100 ± 1) mW/cm^2, monitored by a calibrated silicon reference diode. To determine the external quantum efficiency (EQE) and the mismatch factor, a custom-made setup is used. The monochromatic beam (Oriel Xenon Arc-Lamp Apex Illuminator combined with Cornerstone 260 1/4m monochromator, both Newport, USA) probing the device is chopped and the corresponding current response of the device is measured via a lock-in amplifier 7265 DSP (Signal Recovery, UK). The EQE is measured without extra bias illumination through an aperture of 2.96 mm^2. The long term stability of the organic solar cells is measured in a home built setup using a SOL 1200 (Hönle AG, Germany) sun simulator. All devices were exposed to identical and constant aging conditions: ambient air, Perpendicular illumination with an intensity of 100 mW/cm^2 (the spectrum is similar to AM1.5G) and a temperature of 65 ± 1 °C. Changes in device performance are monitored by recording a current–voltage-curve every two hours and extracting the development of all characteristic parameters as a function of time. A four-point-probe measurement stand S 302–4 (LucasLabs, USA) is used to determine the sheet resistance of the electrodes under ambient conditions. Comparative sheet resistance measurements according to the van der Pauw method led to same results. The transmittance is measured using an Ava-Light-DH-S-Bal (Avantes BV, Netherlands) light source and a CAS 140 CT spectrometer (Instrument Systems GmbH, Germany) through an aperture of 2.96 mm^2. Transmission electron micrographs for top electrode-only samples on a carbon coated copper grid are recorded using a Libra 200 transmission electron microscope (TEM, Carl Zeiss Microscopy GmbH, Germany) with primary electron energy of 200 keV. In the same tool, energy filtered TEM under a collection semi-angle of 12 mrad is measured, with energy steps of 3 eV and a width of the energy slit of 10 eV. Grazing incidence X-Ray diffraction (GIXRD) measurements are carried out in air with a fixed angle of incidence θ of 0.12°, using a D8 Discover device (CuKa-radiation 40 keV, Fa. Bruker AXS, Germany). Scanning electron micrographs of the bended electrodes on PET substrates are recorded using a Zeiss GSM 982 Gemini scanning electron microscope (SEM). Surface scans, height profiles, and roughness of the electrodes without Alq_3 capping layer are determined with a Combiscope atomic force microscope (Aist-NT, Netherlands) in tapping mode. In all cases, several micrographs are recorded at different positions to ensure reproducible results that actually represent the whole sample.

Supporting Information

Supporting Information is available from the Wiley Online Library or from the author.

Acknowledgements

The authors would like to thank the Bundesministerium für Bildung und Forschung (BMBF) in the framework of the InnoProfile Transfer project (03IPT602A) for financial support. Support from the excellence cluster cfaed is gratefully acknowledged. We thank Professor P. Bäuerle from the University Ulm, who pioneered the DCV-5T-Me material system with us and supplied material to the group. We thank Andreas Wendel and Tobias Günther from IAPP for sample preparation, Lutz Wilde from Fraunhofer Center Nanoelektronische Technologien (CNT, Dresden) for XRD measurements, Petr Formanek from the Leibniz-Institut für Polymerforschung (IPF, Dresden) for his great TEM investigations, and Susanne Goldberg from TU Dresden for the SEM measurements.

Received: June 6, 2014
Published online: August 28, 2014

[1] H. Kim, C. M. Gilmore, A. Pique, J. S. Horwitz, H. Mattoussi, H. Murata, Z. H. Kafafi, D. B. Chrisey, *J. Appl. Phys.* **1999**, *86*, 6451–6461.
[2] K. A. Sierros, N. J. Morris, K. Ramji, D. R. Cairns, *Thin Solid Films* **2009**, *517*, 2590–2595.
[3] A. Feltrin, A. Freundlich, *Renew. Energ.* **2008**, *33*, 180–185.
[4] Y. H. Kim, C. Sachse, M. L. Machala, C. May, L. Müller-Meskamp, K. Leo, *Adv. Funct. Mater.* **2011**, *21*, 1076–1081.
[5] J.-Y. Lee, S. T. Connor, Y. Cui, P. Peumans, *Nano Lett.* **2008**, *8*, 689–692.
[6] C. Sachse, L. Müller-Meskamp, L. Bormann, Y. H. Kim, F. Lehnert, A. Philipp, B. Beyer, K. Leo, *Org. Electron.* **2013**, *14*, 143–148.
[7] S. Schubert, J. Meiss, L. Müller-Meskamp, K. Leo, *Adv. Energy Mater.* **2013**, *3*, 438–443.
[8] D. S. Ghosh, L. Martinez, S. Giurgola, P. Vergani, V. Pruneri, *Opt. Lett.* **2009**, *34*, 325–327.
[9] Y.-H. Kim, L. Müller-Meskamp, A. A. Zakhidov, C. Sachse, J. Meiss, J. Bikova, A. Cook, A. A. Zakhidov, K. Leo, *Sol. Energ. Mater. Sol. Cells* **2012**, *96*, 244–250.
[10] A. Kaskela, A. G. Nasibulin, M. Y. Timmermans, B. Aitchison, A. Papadimitratos, Y. Tian, Z. Zhu, H. Jiang, D. P. Brown, A. Zakhidov, E. I. Kauppinen, *Nano Lett.* **2010**, *10*, 4349–4355.
[11] D. S. Hecht, L. Hu, G. Irvin, *Adv. Mater.* **2011**, *23*, 1482–1513.
[12] S. Bae, H. Kim, Y. Lee, X. Xu, J. S. Park, Y. Zheng, J. Balakrishnan, T. Lei, H. R. Kim, Y. I. Song, *Nat. Nanotechnol.* **2010**, *5*, 574–579.
[13] Y. Wang, S. W. Tong, X. F. Xu, B. Özyilmaz, K. P. Loh, *Adv. Mater.* **2011**, *23*, 1514–1518.
[14] Z. Liu, J. Li, Z.-H. Sun, G. Tai, S.-P. Lau, F. Yan, *ACS Nano* **2012**, *6*, 810–818.

[15] Z. Liu, J. Li, F. Yan, *Adv. Mater.* **2013**, *25*, 4296–4301.
[16] Heliatek, press release: Neuer Weltrekord für organische Solarzellen, www.heliatek.com, accessed: March, **2014**.
[17] A. Anctil, C. W. Babbitt, R. P. Raffaelle, B. J. Landi, *Prog. Photovolt: Res. Appl.* **2012**, *21*, 1541–1554.
[18] G. Gu, V. Bulovic, P. E. Burrows, S. R. Forrest, M. E. Thompson, *Appl. Phys. Lett.* **1996**, *68*, 2606–2608.
[19] H. K. Kim, D. G. Kim, K. S. Lee, M. S. Huh, S. H. Jeong, K. I. Kim, T. Y. Seong, *Appl. Phys. Lett.* **2005**, *86*, 183503.
[20] R. S. Sennett, G. D. Scott, *J. Opt. Soc. Am.* **1950**, *40*, 203–211.
[21] J. A. Jeong, H. K. Kim, *Sol. Energy Mater. Sol. Cells* **2009**, *93*, 1801–1809.
[22] M. Fahland, P. Karlsson, C. Charton, *Thin Solid Films* **2001**, *392*, 334–337.
[23] G. Leftheriotis, P. Yianoulis, D. Patrikios, *Thin Solid Films* **1997**, *306*, 92–99.
[24] X. Y. Liu, Y. A. Li, S. Liu, H. L. Wu, H. N. Cui, *Thin Solid Films* **2012**, *520*, 5372–5377.
[25] C. Guillén, J. Herrero, *Thin Solid Films* **2011**, *520*, 1–17.
[26] H. Jin, C. Tao, M. Velusamy, M. Aljada, Y. Zhang, M. Hambsch, P. L. Burn, P. Meredith, *Adv. Mater.* **2012**, *24*, 2572–2577.
[27] S. Schubert, M. Hermenau, J. Meiss, L. Müller-Meskamp, K. Leo, *Adv. Funct. Mater.* **2012**, *22*, 4993–4999.
[28] T. W. Ebbesen, H. J. Lezec, H. F. Ghaemi, T. Thio, P. A. Wolff, *Nature* **1998**, *391*, 667–669.
[29] F. J. Garcia-Vidal, L. Martin-Moreno, T. W. Ebbesen, L. Kuipers, *Rev. Mod. Phys.* **2010**, *82*, 729–787.
[30] W. L. Barnes, A. Dereux, T. W. Ebbesen, *Nature* **2003**, *424*, 824–830.
[31] H. M. Stec, R. A. Hatton, *Adv. Energy Mater.* **2013**, *3*, 193–199.
[32] H. Pang, Y. Yuan, Y. Zhou, J. Lian, L. Cao, J. Zhang, X. Zhou, *J. Lumin.* **2007**, *122*, 587–589.
[33] D. S. Ghosh, N. Formica, T. L. Chen, J. Hwang, C. Eickhoff, V. Pruneri, *Sol. Energy Mater. Sol. Cells* **2013**, *116*, 89–93.
[34] L. Hu, D. S. Hecht, G. Gruner, *Nano Lett.* **2004**, *4*, 2513–2517.
[35] R. Fitzner, E. Mena-Osteritz, A. Mishra, G. Schulz, E. Reinold, M. Weil, C. Körner, H. Ziehlke, C. Elschner, K. Leo, M. Riede, M. Pfeiffer, C. Uhrich, P. Bäuerle, *J. Am. Chem. Soc.* **2012**, *134*, 11064–11067.
[36] E. Voroshazi, B. Verreet, A. Buri, R. Müller, D. Di Nuzzo, P. Heremans, *Org. Electron.* **2011**, *12*, 736–744.
[37] H. Aziz, Z. D. Popovic, S. Xie, A.-M. Hor, N.-X. Hu, C. Tripp, G. Xu, *Appl. Phys. Lett.* **1998**, *72*, 756–758.